APPLIED GEOPHYSICS, Vol.18, No.3 (September 2021), P. 396–407, 9 Figures.
DOI:10.1007/s11770-021-0847-9

Spatiotemporal characteristics and trend assessment of Ms ≥ 5.6 earthquakes in the Tianshan area of China based on co-occurrence analysis and commensurability*

Wan Jia[1,2], Yan Jun-Ping♦[1], Liu Zi-Qiang[2], Wang Xiao-Meng[1], Zhang Yu-Feng[1], and Wang Cheng-Bo[1]

Abstract: Based on the complete seismic data of the Tianshan area in the past 118 years, the co-occurrence rate of earthquakes in different fault zones is calculated, the fault zone with the highest associative degree in the Tianshan area is determined as the research object, extracted the earthquake time series information of the strong associative fault zone and the commensurability method is used to obtain the commensurability expression, the year of strongest earthquake signal is calculated and predicted, then the butterfly structure diagram and commensurability structure system are drawn. Combined the butterfly structure diagram and commensurability structure system to analyze the seismic spatiotemporal structure characteristics of the Tianshan area, judge the trend of future earthquakes, and predict the time of future earthquakes. The results demonstrate that Ms≥5.6 earthquake signals are strong in 2020 and 2021. In order to determine the location of future earthquakes, the historical epicenter migration law of the strongly correlated fault zone in the Tianshan area is analyzed. It is revealed that the epicenter distribution is symmetric in both the longitude and latitude directions. Analyzing the spatial distribution of epicenters, the five successive earthquakes in the strong associative fault zone in the Tianshan area present a pentagonal symmetrical structure in space. It is judged that the next earthquake will migrate toward the northeast. Additionally, the sunspot has a strong seismic correlation with the strong associative fault zone in the Tianshan area. Specifically, on the 11-year cycle scale of sunspot activity, 64.71% of earthquakes occurred in the fluctuation descending range; on the monthly scale of sunspot activity. Hence, it has been verified that the proposed disaster prediction method based on commensurability theory is scientific and has a broad application prospect.
Keywords: Tianshan area, earthquake, associative degree, commensurability

Introduction

According to the 2020 Global Risks Report, the Earth will face severe threats from natural disasters over the coming decade (World Economic Forum, 2020). Earthquakes, which are described as "the most serious disaster among all calamities," are sudden events that cause great destruction (Qin et al., 2011).

Manuscript received by the Editor June 21, 2019; revised manuscript received December 21, 2020
* This work was supported by the National Natural Science Fund of China (grant number 41877519)
1. School of Geography and Tourism, Shaanxi Normal University, Xi'an 710119, China.
2. North Minzu University, Yinchuan, Ningxia 750021, China.
♦Correspondence: Yan Jun-ping (E-mail: yanjp@snnu.edu.cn).

Strengthening earthquake disaster prediction is not only the basic connotation of adapting to global changes, but also an inevitable requirement for improving the ability of cities to resist earthquake disaster risks, boost emergency response, and achieve regional sustainable development (Yan, 2013).

The methods of earthquake prediction primarily include precursor statistical method and information statistical method. Precursor statistical method based on physical observation data captures the weak signal of earthquake precursor by capturing observation data such as stress field change (Qiang et al., 2008), infrared anomaly (Wei et al., 2008), fluid characteristic value (Chen et al., 2018), electromagnetic anomaly value (Tu et al., 2019) and b-value before the earthquake (Meng et al., 2021), and then predicts the time of the earthquake. However, this method lacks universal applicability for earthquake prediction due to the limitation of the distribution density of observation stations, the length of station construction time, and the observation approaches. Compared with the precursory statistics method, the information statistics method has the characteristics of simple calculation and fast calculation. The creation of commensurability theory was based on the commensurability in astronomy. Weng (1984) developed the theory of commensurability in theory and practice through the method of information statistics, and put forward a disaster prediction method based on commensurability theory. This method omits the detailed data of random events, simplifies the random variables to BOOL symbols, and describes its statistical law in time series. Then there was the triplet character method on the basis of commensurability (Hu and Han, 2005; Guo et al., 2006, 2016; Guo and Guo, 2017). Yan (2016) made several successful achievements in the assessment of the trends of natural disasters by using information forecasting theory. The accuracy of trend prediction has reached 61.5% (Liu and Yan, 2015).

Non-natural disaster events form and evolve independently. Relevant studies have reported a certain correlation among ground motion parameters (Wu and Cao, 2018), stress field features (Shan et al., 2015), seismic focus parameters (Guilherme and Aderson, 2018), and energy release process (Li, 2019) in different seismic field points within a certain area, that is, a phenomenon of synchronous fluctuation between seismic activities. Existing studies have taken typical fault zones or block areas as the research object while ignoring the triggering between seismic activities, affecting the accuracy of the prediction results. The co-occurrence analysis method can realize this correlated visualization through recursive induction of seismic statistics and by establishing a network model and identifying the internal links between earthquakes in different area. This method reveals regular earthquake occurrence from surface phenomena to internal association, thereby providing a new idea for optimizing the assessment of earthquake occurrence trends.

The current study uses the co-occurrence analysis method and commensurability information in combination with a butterfly diagram and commensurability structure system to analyze the characteristics of earthquake distribution and assess the earthquake occurrence trend. This work was realized based on the complete seismic data of the Tianshan area in the past 118 years. This work provides a solid reference basis reference basis for regional earthquake disaster prevention and mitigation work.

Areal descriptions

The Tianshan Orogenic belt is one of the most active intracontinental orogenic belts in the world and is the largest regenerative orogenic belt in Eurasia. This belt is located on the suture zone of the Tarim plate and Kazakhstan plate, which consists of the Tarim plate, Ili microplate, and Jungar microplate (Deng et al., 2000). In the late Cenozoic period, the Indian Ocean and Eurasian plates continued to squeeze northward following the collision in the

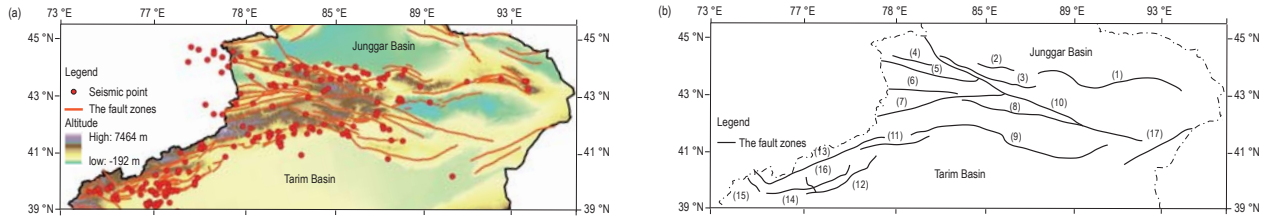

Figure 1. Active tectonic map (a) and schematic of fault structure (b) of Tianshan area in China. Fig. 1b was drawn according to Feng's research (Feng 1986a; 1986b). Fault zones: (1) Bogda–Karlik, (2) Khorgos–Tuguli, (3) Tuosite–Toutunhe, (4) Kusongmuqieke, (5) Kashgar River, (6) Qiahepuhe, (7) Nalati–Haerke, (8) Kekendaban, (9) North Bugur–Xingeer, (10) Borohoro–Yilianhabierga, (11) Qiulitage, (12) Kalpin, (13) Kokshal, (14) Yisilake–Kalawuer, (15) Fergana, (16) Puchang, and (17) Sailikeshayi.

Himalayas, thereby causing crustal deformation in the Tianshan area. Moreover, the orogenic block rapidly uplifted and formed a regenerated orogenic belt. The orogenic belt was reversely pushed toward the north and south, resulting in the formation of a depression basin, active reverse faults, and active folds in the Tianshan area (Figure 1a). According to the study by Feng (Feng, 1986a, b), the Tianshan area is divided into 17 fault zones, which comprise its basic tectonic image (Figure 1b).

Statistics show that seismicity in the Tianshan area is frequent, with 41 Ms ≥ 6.0 earthquakes occurring from 1900 to 2017; of this number, eight were Ms ≥ 7.0 earthquakes. This area is rich in ice water, minerals, and forest grassland resources, which are the foundation for agricultural production and economic activities in the region. It also has a high concentration of cities.

Methods

Co-occurrence analysis

(1) Data

The seismic data from 1900 to 2010 are from the Global Earthquake Catalogue edited by Song et al. (2011). The seismic data from 2011 to 2018 are from the Earthquake Hazards Program (USGS, https://earthquake.usgs.gov/). The relative numbers of monthly sunspot activity are from the National Centers for Environmental Information (NCEI, https://www.ncei.noaa.gov/).

(2) Establishment of the network model

A total of 17 fault zones in the Tianshan area are selected as the study subjects. Any two fault zones are bidirectionally linked with dashed lines. The simultaneous frequency of earthquakes between fault zones is obtained during a certain year, the year before, and the year after. We convert the edge lines between the associated objects into full lines and remove the dashed lines between unrelated objects. Then, the network model of the Tianshan area is established.

We define associative degree between network nodes, G denotes the associative degree network model of the Tianshan area, which is a two-tuple model with constituent elements, including the nonempty set V(G) = {*vi*}, E(G) = {*ek, e'l*} (Wu et al., 2010). Element *vi* in V(G) represents a node, that is, a fault zone. In E(G), element *ek* represents a real edge, and *e'l* represents a virtual edge. If $ek = (v_i, v_j)$, then *ek* is a real edge and *ek* represents a fault zone *i* pointing to the fault zone *j*.

A*v* represents the G incidence matrix. The node number is *v*, and the edge number is *e*, which is a $v \times v$ order matrix. When A$v = [a_{ij}]$, $i \in (1,v)$, $j \in (1,v)$, a_{ij} represents the associative degree between nodes v_i and v_j (Hu, 2013).

The associative degree is defined as the sum of the weights between nodes. If the degree is 0, then the node is isolated and associated with no node in the network.

(3) Salton index

Associative degree refers to the percentage of two things related to each other and is usually characterized by co-occurrence rate, i.e. index. the well-known associative degree include that of Jaccard, Salton's cosine, and that of Dice et al. (Eck and Waltman, Egghe (2009) compared these measures and concluded that all other algorithms, except Jaccard's measurement, have a linear correlation with Salton's cosine. The revised Salton's cosine showed that it was more sensitive than Jaccard's in reflecting the accuracy of associative degree (Salton and McGill, 1983; Morillo et al.,2003; Hu et al., 2014). Therefore, the revised Salton's cosine was selected to calculate the co-occurrence rate of earthquake disaster among the fault zones in this study. The revised Salton's cosine, denoted as S, is defined as.

$$Sij = \frac{Cij}{\sqrt{Ci \times Cj}} - \frac{Cij^2}{Ci \times Cj},$$

where *Sij* denotes Salton's cosine between fault zones *i* and *j*. *Cij* denotes the earthquake co-occurrence frequency during a certain year, the year before, and the year after between any two fault zones *i* and *j*. *Ci* and *Cj* are the total numbers of earthquakes in fault zones *i* and *j*, respectively.

Commensurability information

Commensurability was first proposed by Bode (1747–1826) and Titius (1729–1796) to describe the distance of planetary motion in the solar system. Weng (1984) applied this concept to information prediction. Commensurability is an expression of the cyclical expansion of natural orders. This expression is a mixed hypothesis of the superposition of cycles in different lengths, and an expression of the principles can jointly measure the elements of one system (Yan, 2016). The basic principle is that several relation sets exist in the time series of disaster events or abnormal signals. When the frequency of one relational expression is relatively high, the relational expression rule can reflect a certain cycle. Commensurability relational expressions include ternary, quaternary, and pentabasic commensurability; they can calculate the timing of the next disaster event by using the existing time series of disaster events. To avoid repetition herein, we only provide the ternary,

quaternary, and pentabasic commensurability relational expressions, the specific derivation process is available in the reference (Lv and Zhang, 1996).

The relational expression for ternary commensurability is $Yd = Ya + Yb - Yc$, $a + b - c = d$; and the relational expression for quaternary commensurability is $\Delta Y = Ya + Yb - Yc - Yd$, $a + b = c + d$. If the year in which the next disaster event will occur is denoted as *Yi*. the year in which the last disaster event occurred is *Yj*. Then, $Yi = Yj + \Delta Y$; The relational expression for pentabasic commensurability is $Yf = Ya + Yb + Yc - Yd - Ye$, $f = a + b + c - d - e$. Here, *a, b, c, d, e, f* indicates the time series number of the year in which the earthquake occurred; *Ya, Yb, Yc, Yd, Ye, Yf* represent the *a, b, c, d, e, f* years in which the earthquake occurred in the earthquake time series; *Yi* denotes the year in which the earthquake is predicted.

Seismic associative analyses of Tianshan area

Construction of co-occurrence matrix

A total of 203 Ms ≥ 4.2 earthquakes have occurred in the Tianshan region since the start of the 19th century. The frequencies of the occurrence of earthquakes during a certain year, the year before, and the year after are obtained between any two fault zones. Then, the co-occurrence frequency of two-fault zone earthquakes can be obtained. Through this method, the 17 × 17 co-occurrence symmetric matrix for the Tianshan area is constructed (Table 1).

The data on the diagonal part of the co-occurrence matrix refer to the number of earthquakes occurring in any one fault zone. The data on the nondiagonal part denote the number of earthquakes between corresponding fault zones. On the basis of the co-occurrence matrix, the number of earthquake co-occurrence frequencies in each fault zone can be obtained. The internal association of earthquake occurrence in different fault zones can subsequently be inferred.

Calculation of relative associative degree

The co-occurrence matrix stores the frequency of earthquake co-occurrence in different fault zones and shows the apparent characteristics of statistical data. However, this matrix inaccurately expresses the degree of association between any two fault zones. The revised Salton's cosine can be used to express the degree of interaction between these zones. Calculating the revised Salton's cosine between any two different fault zones of the Tianshan area shows that when the value is high, the interaction degree is strong; when the value is low, the

Table 1. Co-occurrence matrix of earthquakes in different fault zones of the Tianshan area.

Sequence of fault zones	(1)	(2)	(3)	(4)	(5)	(6)	(7)	(8)	(9)	(10)	(11)	(12)	(13)	(14)	(15)	(16)	(17)
(1)	15	2	2	1	4	4	5	3	6	6	2	5	3	4	4	7	5
(2)	2	5	1	1	2	3	3	2	4	2	2	3	3	2	3	3	3
(3)	2	1	11	3	3	2	3	2	9	3	0	9	6	4	3	5	3
(4)	1	1	3	9	6	3	2	2	6	1	1	6	4	3	4	4	2
(5)	4	2	3	6	16	4	6	4	9	2	2	8	6	4	4	5	3
(6)	4	3	5	3	4	7	3	3	7	4	2	4	3	3	3	5	6
(7)	5	3	3	2	6	3	10	4	9	4	3	9	6	4	4	5	5
(8)	3	2	2	2	4	3	4	7	6	3	3	6	2	4	2	3	5
(9)	6	4	9	6	9	7	9	6	30	7	6	19	15	7	9	12	9
(10)	6	2	3	1	2	4	4	3	7	9	1	8	6	3	4	5	6
(11)	2	2	0	1	2	2	3	3	6	1	8	5	4	2	2	2	4
(12)	5	3	9	6	8	4	9	6	19	8	5	31	13	8	7	9	7
(13)	3	3	6	4	6	3	6	2	15	6	4	13	12	3	5	8	6
(14)	4	2	4	3	4	3	4	4	7	3	2	8	3	9	4	3	4
(15)	4	3	3	4	4	3	4	2	9	4	2	7	5	4	8	4	4
(16)	7	3	5	4	5	5	5	3	12	5	2	9	8	3	4	10	6
(17)	5	3	3	2	3	6	5	5	9	5	4	7	6	4	4	6	6

Annotation of fault zone sequence in Table 1: (1) Bogda–Karlik, (2) Khorgos–Tuguli, (3) Tuosite–Toutunhe, (4) Kusongmuqieke, (5) Kashgar River, (6) Qiahepuhe, (7) Nalati–Haerke, (8) Kekendaban, (9) North Bugur–Xingeer, (10) Borohoro–Yilianhabierga, (11) Qiulitage, (12) Kalpin, (13) Kokshal, (14) Yisilake–Kalawuer, (15) Fergana, (16) Puchang, and (17) Sailikeshayi.

interaction degree is weak.

When establishing the associative degree network model of fault zones in the Tianshan area (Figure 2), each node corresponds to the fault zone (Table 1), and the width of the full line visualizes the associative degree between any two nodes. When the line is wide, the associative degree is strong; when the line is fine, the associative degree is weak. The number between the nodes is the value of the revised Salton's cosine.

By analyzing the associative degree network model of fault zones in the Tianshan area, we identify the fault zones of Tuosite–Toutunhe, Qiahepuhe, Nalati–Haerke, Borohoro–Yilianhabierga, Puchang, and North Bugur–Xingeer as the core nodes. The associative degrees among Tuosite–Toutunhe and North Bugur–Xingeer, Qiahepuhe and Borohoro–Yilianhabierga, and Nalati–Haerke and Puchang are the strongest with a 25% rate of the earthquakes' co-occurrence. No connecting edge between Tuosite–Toutunhe and Qiulitage exists, and the associative degree between the two fault zones is the weakest at 0% of the earthquakes' co-occurrence.

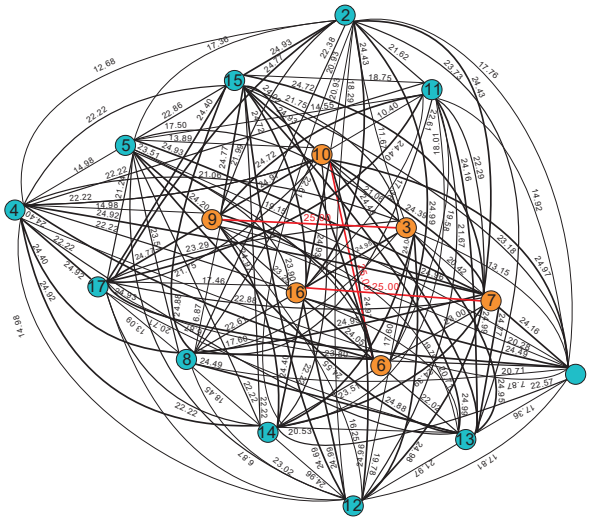

Figure 2. Associative degree network model of fault zones in the Tianshan area.

Temporal symmetry and trend assessment

Commensurability calculation

The co-occurrence analysis results show that the associative degrees between Tuosite–Toutunhe and North Bugur–Xingeer, between Qiahepuhe and Borohoro–Yilianhabierga, and between Nalati–Haerke and Puchang are the strongest. Therefore, we assess these six fault zones in the Tianshan area with their earthquake occurrence trends. For convenience, we refer to the six fault zones as the Tianshan fault zone with strong associative degrees.

Extracting the year of earthquake occurrence from

Table 2. Catalog of Ms ≥ 5.6 in the Tianshan fault zone with strong associative degrees in 1920–2018.

No.	Date (year-month-day)	Epicenter location		Magnitude (Ms)	Locality
		Latitude	Longitude		
1	1921	43.90	81.40	6.5	Ili, Xinjiang, China
2	1944-3-9	44.00	84.00	7.1	Xinyuan, Xinjiang, China
3	1949-2-23	42.00	84.00	7.3	Kuqa, Xinjiang, China
4	1955-4-24	44.20	83.60	6.5	Usu, Xinjiang, China
5	1972-4-9	42.30	84.80	5.6	Bugur, Xinjiang, China
6	1973-6-2	44.14	83.59	5.6	Jinghe, Xinjiang, China
7	1976-1-10	42.20	83.30	5.8	Kuqa, Xinjiang, China
8	1979-3-29	42.00	83.40	6	Kuqa, Xinjiang, China
9	1980-11-6	43.81	86.14	5.7	Manas, Xinjiang, China
10	1987-1-5	41.95	81.31	5.9	Baicheng, Xinjiang, China
11	1990-10-24	44.22	83.95	5.6	Jinghe, Xinjiang, China
12	1995-9-26	41.85	81.64	5.8	Baicheng, Xinjiang, China
13	2003-12-1	42.96	80.71	6.1	Zhaosu, Xinjiang, China
14	2007-7-20	42.90	82.40	5.7	Ili, Xinjiang, China
15	2011-11-1	43.65	82.44	5.6	Nilka, Xinjiang, China
16	2013-1-29	42.60	79.70	6.1	Kazakhstan
17	2013-3-29	43.40	86.80	5.6	Urumqi, Xinjiang, China
18	2016-12-8	43.83	86.35	6.2	Hutubi, Xinjiang, China
19	2017-9-16	42.11	83.43	5.7	Aksu, Xinjiang, China

Table 2 shows that 19 Ms ≥ 5.6 earthquakes occurred in the Tianshan fault zone with strong associative degrees starting in 1920. Two such earthquakes occurred in 2013, and they were recorded as one earthquake in the time series. The time series information is extracted to verify the commensurability of the 19 earthquakes. Commensurability is found to be significant, that is, more than nine groups of commensurable equations are identified for each year. The commensurability in 1979 was the strongest with 22 commensurability equations (Figure 3).

The commensurability of the Ms ≥ 5.6 earthquakes in the Tianshan area is calculated as follows: Y_1 = 1921, Y_2 = 1944, Y_3 = 1949, Y_4 = 1955, Y_5 = 1972, Y_6 = 1973, Y_7 = 1976, Y_8 = 1979, Y_9 = 1980, Y_{10} = 1987, Y_{11} = 1990, Y_{12} = 1995, Y_{13} = 2003, Y_{14} = 2007, Y_{15} = 2011, Y_{16} = 2013, Y_{17} = 2016, Y_{18} = 2017, Y_{19} = ?. The next earthquake occurrence is Y_{19}, which can be calculated on the basis of the annual time series.

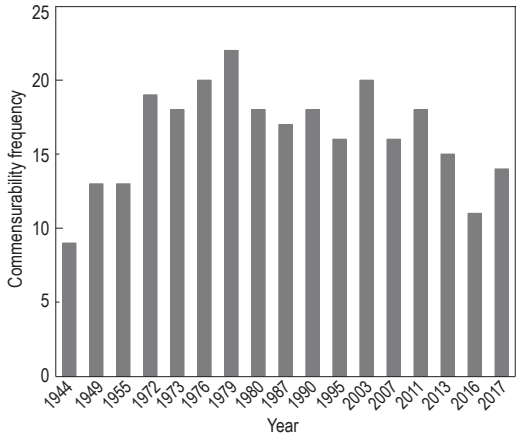

Figure 3. Commensurability verification diagram of Ms ≥ 5.6 earthquake time series in Tianshan area.

The relational expression of ternary commensurability is $Y_{19} = Ym + Yn - Yp$, m + n − p = 19. The results for the earthquake occurrence are as follows: eight times in 2020; seven times in 2024; six times in 2034; five times in 2022; and four times in 2021, 2025, and 2031.

The relational expression of quaternary commensurability is $Y_{19} = Y_{18} + \Delta Y$, $\Delta Y = Ya + Yb - Yc - Yd$, a + b = c + d. The results are as follows: 37 times in 2021, 30 times in 2020, 28 times in 2022, 28 times in 2023, 20 times in 2026, 18 times in 2024, 17 times in 2025, and 17 times in 2027.

The relational expression of pentabasic commensurability is Y19 = Ya + Yb + Yc − Yd − Ye,

19 = a + b + c − d − e. The results are as follows: 82 times in 2020, 71 times in 2021, 76 times in 2022, 63 times in 2023, 62 times in 2024, 49 times in 2025, 52 times in 2026, and 48 times in 2027.

Table 3 shows the frequency of earthquake occurrence in the next decade that is calculated by commensurability methods. The years 2020 and 2021 have the strongest signals, indicating that an Ms ≥ 5.6 earthquake will occur in the Tianshan fault zone with strong associative degrees in either one of these periods.

Table 3. Commensurability frequencies of Ms ≥ 5.6 earthquake in the Tianshan fault zone with strong associative degrees.

	2020	2021	2022	2023	2024	2025	2026	2027	2028	2029
Ternary	8	4	5	2	7	4	2	2	2	3
Quaternary	30	37	28	28	18	17	20	17	11	8
Pentabasic	82	71	76	63	62	49	52	48	46	37

Butterfly diagram trend assessment

The butterfly structure diagram is a further extension of the commensurability method and is used to reflect the time symmetric structure of natural disasters, namely, the characteristics of a set of disaster time series with equal time intervals (Arlt, 2009; Cristo et al., 2011). The butterfly diagram constructed for the period of 1920–2021 in the Tianshan fault zone with strong associative degrees and the seismic time series exhibit an evident symmetrical characteristic (Figure 4). Three groups of cycles, namely, 4/40/41, relate to 2020. Six cycles, namely, 4/8/27/31/34/41, relate to 2021.

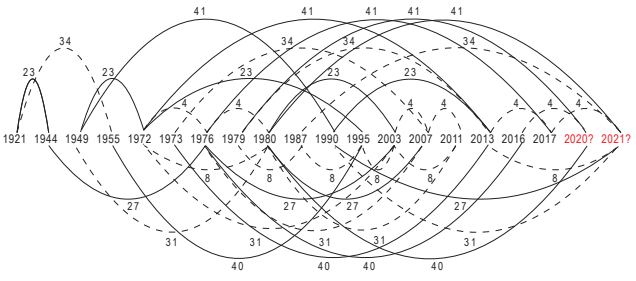

Figure 4. Butterfly diagram of Ms ≥ 5.6 earthquake in the Tianshan fault zone with strong associative degrees.

The random probability of the butterfly diagram is $P = N / T$, and the prediction confidence level is $(1 - a) = N / (T + 1)$. P is the probability of the assessment year in the time series of earthquake events, T is the total number of earthquake events, and M is the number of events involved in the actual forecast, that is, the year statistics associated with the main cycle (Yan et al. 2011) . The random probability in 2020 is 61.11%, and that in 2021 is 88.89%. The prediction confidence level is 57.89% in 2020 and 84.21% in 2021. Therefore, an Ms ≥ 5.6 earthquake will occur in the Tianshan fault zone with strong associative degrees in 2020 or 2021.

Commensurability structure system

The commensurability structure system is another approach to expressing the temporal symmetry of natural disaster events, and it can reflect their mutual order and temporal rhythm (Weng, 1984). Figure 5 presents the commensurability structure system in the Tianshan fault zone with strong associative degrees. The figure intuitively shows an evident symmetry in time in the area. The main cycles are 4a/23a, and the least important cycle is 11a in the thwartwise direction. As for the longitudinal direction, the main cycles are 10a/31a, and the less important cycles are 3a/28a. On the basis of the principle of time translation symmetry, the years 2020 and 2021 are found to be the periods in which earthquakes may occur. The results are consistent with the conclusions of the commensurability calculation and assessment of the butterfly structure diagram.

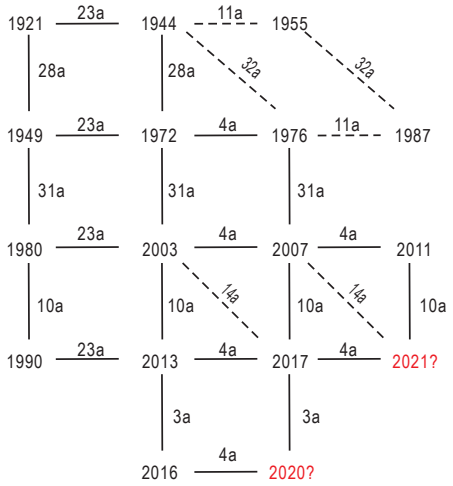

Figure 5. Commensurability structure system of Ms ≥ 5.6 earthquakes in the Tianshan fault zone with strong associative degrees.

Spatial symmetry and trend assessment

Epicenter pentagonal symmetric structur

We analyze the spatial activity characteristics of Ms ≥ 5.6 earthquakes in the Tianshan fault zone with strong associative degrees and mark the epicenters in accordance with the annual time series of the earthquakes (Table 2). Two earthquakes occurred in 2013. One occurred in Kazakhstan, and the epicenter was located in the Nalati–Haerke fault zone. The other one occurred in Urumqi, and the epicenter was located in the Borohoro–Yilianhabierga fault zone. These earthquakes have different fault zones; thus, they are respectively space tagged. We derive the five successive earthquakes as a group and link their epicenters with straight lines (Figure 6). The time series is divided into four pentagon groups.

By analyzing the epicenters' spatial locations, we find a northeast–southwest strike of the symmetry axis given by Y = 0.1015X + 34.95. As shown in Figure 6, the epicenters regularly obey the distribution of "two and three" on both sides of the symmetry axis. Epicenters No. 1, No. 2, and No. 4 in group one are above the symmetry axis; whereas No. 3 and No. 5 are under the symmetry axis. A similar pattern is noted in group two, in which epicenters No. 6 and No. 9 are also above the symmetry axis; whereas No. 7, No. 8, and No. 10 are under the symmetry axis. Epicenters No. 11 and No. 15 in group three are above the symmetry axis; whereas No. 12, No. 13, and No. 14 are under the symmetry axis. Group four is incomplete because the three epicenters are distributed below the symmetry axis (No. 16, No. 17, and No. 19). Therefore, the assessment results indicate that the next earthquake will occur above the symmetry axis.

Latitudinal and longitudinal epicenter migration

Figure 7a shows the Ms ≥ 5.6 earthquake epicenter migrations in the latitudinal direction while Figure 7b presents those in the longitudinal direction in the Tianshan fault zone with strong associative degrees. The epicenters' migration in the latitudinal direction is 43.5° N is the symmetry axis (Figure 7a). The epicenters also regularly show "two and three" on the two sides of the symmetry axis, that is, two epicenters located on one side of the symmetry axis, three epicenters located on another one. In group one, the earthquakes that occurred

in 1921, 1944, and 1955 are located in the north side of 43.5° N; those that occurred in 1949 and 1942 are located in the south side. In group two, the earthquakes that occurred in 1973 and 1980 are located in the north side of 43.5° N; those that occurred in 1976, 1979, and 1987 are located in the south side. In group three, the earthquakes that occurred in 1990 and 2011 are located in the north side of 43.5° N; those that occurred in 1995, 2003, and 2007 are located in the south side. Group four is incomplete because of three earthquakes (two in 2013 and one in 2017) that occurred in the south side of the symmetry axis and one earthquake in 2016 that occurred in the north side of the symmetry axis. Therefore, the "two and three" patterns are regularly combined, and the next epicenter is projected to be in the north of the 43.5° N latitude.

The epicenter migration in the longitudinal direction is at 81.5° E in the symmetry axis (Figure 7b). The epicenter regularly shows the "one west and four east" pattern on its two sides, that is, the epicenter in any group regularly obeys the distribution with one epicenter in the west side of the symmetry axis and four epicenters in the east side. In group one, the earthquakes that occurred in 1921 are located in the west side of 81.5° E; those that occurred in 1944, 1949, 1955, and 1972 are located in the east side. In group 2, the earthquakes that occurred in 1987 are located in the west side of 81.5° E; those that occurred in 1973, 1976, 1979, and 1980 are located in the east side. In group three, the earthquake in 2003 is located in the west side of 81.5° E; those that occurred in 1990, 1995, 2007, and 2011 are located in the east side. Group four is incomplete because of an earthquake (2013) that occurred in the west side of the symmetry axis and three earthquakes (2013, 2016, and 2017) that occurred in the east side of the symmetry axis. Therefore, the "one west and four east" patterns are regularly combined, and the next epicenter is projected at the east side of 81.5° E longitude.

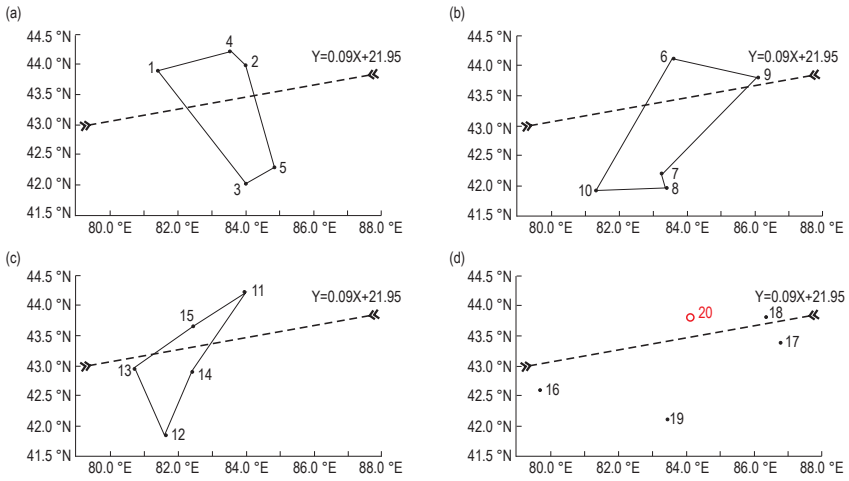

Figure 6. Spatial symmetry structures of Ms ≥ 5.6 earthquakes in the Tianshan fault zone with strong associative degrees: (a) group one, (b) group two, (c) group three, and (d) group four.

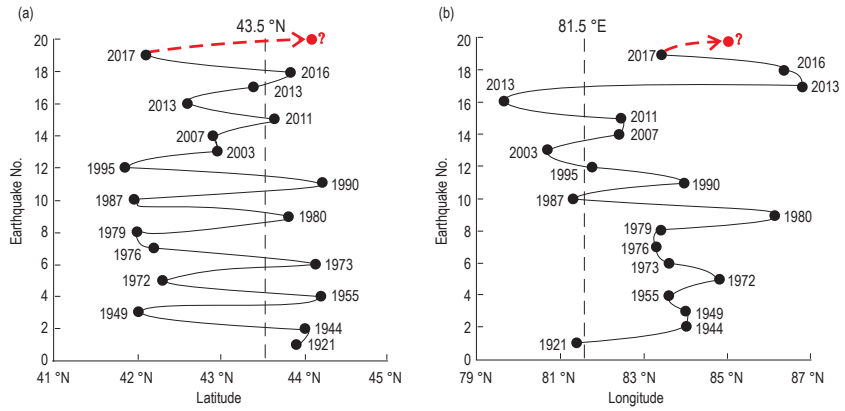

Figure 7. (a) Latitudinal and (b) longitudinal epicenter migration of Ms ≥ 5.6 earthquakes in the Tianshan fault zone with strong associative degrees.

Relationship between sunspot activity and earthquake

Solar activity is related to the frequency and energy distribution of earthquakes. The effect of solar activity on seismic activity is mainly realized by the electromagnetic effect (Jiang, 1985; Yin et al., 2011). When the sunspot activity is enhanced or weakened, the magnetic storm activity increases or decreases accordingly, thus leading to the corresponding enhancement or diminution of the Earth's current. The Earth's current causes changes in its internal temperature; thus, rock temperature changes correspondingly. The changes generate a spontaneous magnetostrictive effect, which causes rock volume deformation and creates additional stress in the rock. These conditions trigger an earthquake.

A strong correlation exists between the sunspot activity cycle and the year in which earthquakes occurred in the Tianshan fault zone with strong associative degrees (Figure 8). The sunspot circumferential phase can directly reflect the influence of solar activity on earthquake activity (Fang et al., 2003), that is, this phase records the instance when the peak value of the sunspot activity cycle is 180°, the valley value before peak is 0°, and the valley value after peak is 360°. Used the phase angle to express earthquake that occurred in its respective year information, and the result is associated with the sunspot circumferential phase (Table 4). The phase angle is denoted as α. If $\alpha \in [0°,180°]$, then the earthquakes occurred at the ascending interval in a sunspot activity. If $\alpha \in (180°,360°]$, then the earthquakes occurred at the descending interval in a sunspot activity. Statistics show that 35.29% of Ms ≥ 5.6 earthquakes in the Tianshan fault zone with strong associative degrees

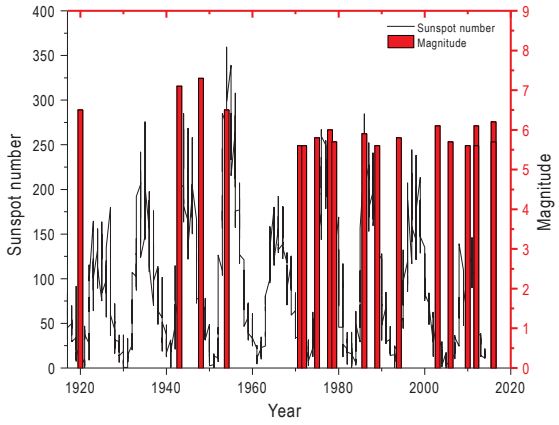

Figure 8. Corresponding relationship of time between sunspot yearly scale cycle and Ms ≥ 5.6 earthquakes in the Tianshan fault zone with strong associative degrees.

Table 4. Sunspot circumferential phases corresponding to the years of Ms ≥ 5.6 earthquakes in the Tianshan fault zone with strong associative degrees.

No.	Date (year-month-day)	Magnitude (Ms)	Locality	Phase angle (α°)
1	1921	6.5	Ili, Xinjiang, China	296.62°
2	1944-3-9	7.1	Xinyuan, Xinjiang, China	360.00°
3	1949-2-23	7.3	Kuqa, Xinjiang, China	204.66°
4	1955-4-24	6.5	Usu, Xinjiang, China	48.29°
5	1972-4-9	5.6	Bugur, Xinjiang, China	261.22°
6	1973-6-2	5.6	Jinghe, Xinjiang, China	291.95°
7	1976-1-10	5.8	Kuqa, Xinjiang, China	360.00°
8	1979-3-29	6	Kuqa, Xinjiang, China	155.45°
9	1980-11-6	5.7	Manas, Xinjiang, China	211.50°
10	1987-1-5	5.9	Baicheng, Xinjiang, China	28.24°
11	1990-10-24	5.6	Jinghe, Xinjiang, China	184.93°
12	1995-9-26	5.8	Baicheng, Xinjiang, China	330.41°
13	2003-12-1	6.1	Zhaosu, Xinjiang, China	248.33°
14	2007-7-20	5.7	Ili, Xinjiang, China	320.00°
15	2011-11-1	5.6	Nilka, Xinjiang, China	91.64°
16	2013-1-29	6.1	Kazakhstan	137.45°
17	2013-3-29	5.6	Urumqi, Xinjiang, China	144.00°
18	2016-12-8	6.2	Hutubi, Xinjiang, China	?
19	2017-9-16	5.7	Aksu, Xinjiang, China	?

occurred at the ascending interval in the sunspot activity cycle and that 64.71% occurred at the descending interval in the sunspot activity cycle.

The correlation between the Ms ≥ 5.6 earthquakes' occurrence time in the Tianshan fault zone with strong associative degrees and the monthly sunspot cycle scale is analyzed (Figure 9). The monthly sunspot number was recorded until June 2017. The Ms5.7 earthquake that occurred on 16 September 2017 in Aksu is not within the scope of the statistics. As shown in Figure 9, 13 earthquakes that occurred in the sunspot monthly scale cycle showed extreme values and accounted for 72.22% of the total number in the Tianshan fault zone with strong associative degrees. Another five earthquakes that occurred within the monthly scale cycle had insignificant values, and the proportion is 27.78%. Two of these earthquakes (1955-4 Ms6.5, 2013-3 Ms5.6) occurred in the ascending arc of the sunspot monthly scale cycle. The other three earthquakes (1973-6 Ms5.6, 2003-12 Ms6.1, and 2007-7 Ms5.7) occurred in the descending arc of the scale cycle. The cycle predicted by Bhowmik and Nandy (2018) has been provided that the year 2020/2021 would be near the trough of the 24th sunspot activity cycle and that the probability of earthquakes in the Tianshan region is relatively high, further validating the results of the previous study.

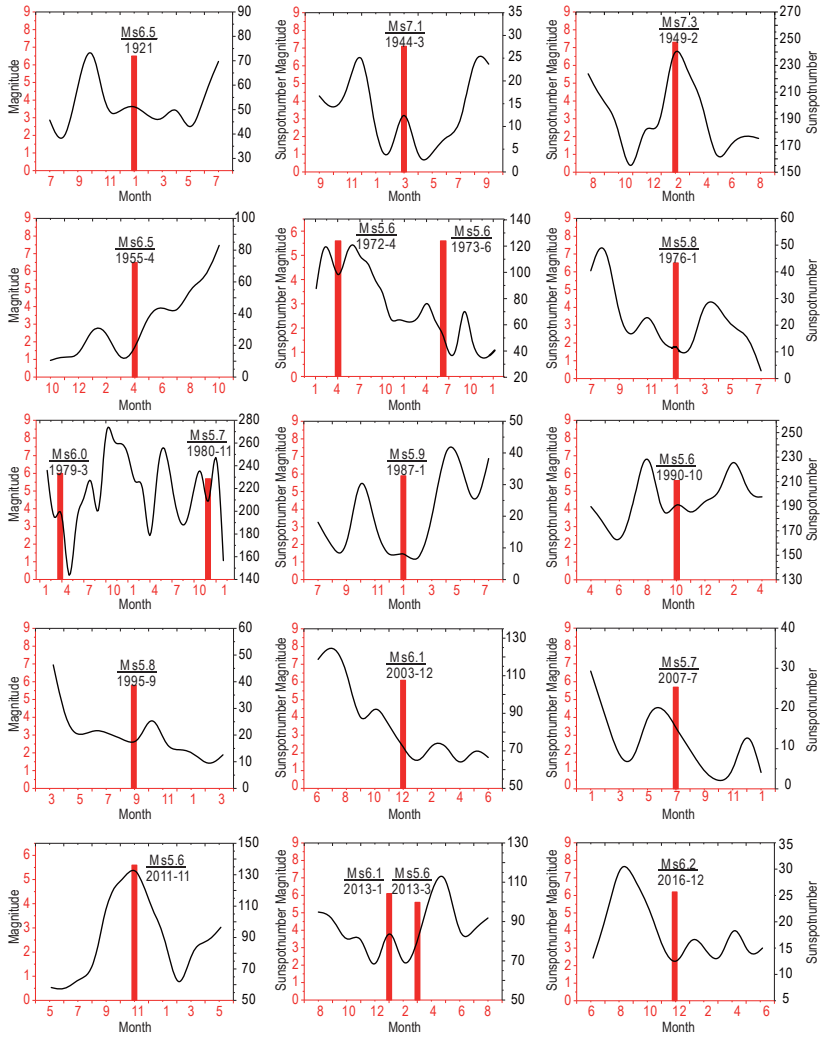

Figure 9. Correlation between Ms ≥ 5.6 earthquakes in the Tianshan fault zone with strong associative degrees and the sunspot monthly scale cycle.

Discussion

Commutability is an effective disaster prediction method, and a considerable number of successful cases have been obtained (Long et al., 2006; Zhang et al., 2012; Cui et al., 2013; Wang et al., 2018). In this study, 17 fault zones in the Tianshan area were taken as the research objects. The co-occurrence analysis method and commensurability method were used to judge the future trend of earthquake occurrence in the Tianshan area. Moreover, the scientific question of "Where? When? What magnitude?" was answered. In sum, two issues require further improvement and exploration in future research:

1) Noise signal processing. The commensurability method belongs to the category of information prediction. The presence of noise signals is the cause of errors in prediction results. Thus, how to effectively identify and eliminate noise signals in the disaster time series is a crucial issue that needs to be addressed to improve the accuracy of the commensurability method.

2) Docking of symmetry mechanism of time and space. Are time symmetry in statistical law and spatial symmetry in epicenter migration mutually sufficient and necessary? How can the statistical law of seismic appearance be correlated with the internal shaking force? These questions need further investigation in the future.

Conclusions

By establishing the associative degree network model of fault zones in the Tianshan area, this study finds the fault zones of Tuosite–Toutunhe, Qiahepuhe, Nalati–Haerke, Borohoro–Yilianhabierga, Puchang, and North Bugur–Xingeer as core nodes. The associative degrees between Tuosite–Toutunhe and North Bugur–Xingeer,

between Qiahepuhe and Borohoro–Yilianhabierga, and between Nalati–Haerke and Puchang are the strongest at 25%. The associative degrees between Tuosite–Toutunhe and Qiulitage are the weakest with 0 value.

The year information about Ms ≥ 5.6 earthquakes in the Tianshan fault zone with strong associative degrees in the recent century has good commensurability. In the calculation of ternary, quaternary, and pentabasic commensurability, the occurrences of Ms ≥ 5.6 earthquakes in 2020 and 2021 have the strongest signals. The random probabilities of a Ms ≥ 5.6 earthquake occurring in 2020 and 2021 are 61.11% and 88.89%, respectively. The 2020 and 2021 prediction confidence levels are 57.89% and 84.21%, respectively. The results analyzed by the butterfly diagram and commensurability structure system are consistent with the commensurability calculations.

The Ms ≥ 5.6 earthquake in the Tianshan fault zone with strong associative degrees has good spatial pentagonal symmetric structure. The symmetry axis is a northeast–southwest strike, and its equations is Y = 0.1015X + 34.95. The epicenters in each group regularly obey the "two and three" distribution on both sides of the symmetry axis. The epicenter distribution in the latitudinal direction is 43.5° N in the symmetry axis. The epicenter distribution in the longitudinal direction is 81.5° E as the symmetry axis. The epicenters regularly show a "one west and four east" distribution on both sides of the symmetry axis. The next epicenter may migrate toward the northeast (i.e., north of 43.5° N and east of 81.5° E).

The sunspot activity cycle and timing of earthquake occurrences in the Tianshan fault zone with strong associative degrees are strongly correlated. On the scale of the 11-year cycle of sunspot activity, 35.29% and 64.71% of the Ms ≥ 5.6 earthquakes in the Tianshan fault zone with strong associative degrees occurred at ascending and descending intervals in the sunspot activity cycle, respectively.

References

Arlt, R., 2009, The butterfly diagram in the eighteenth century: Solar Physics, **255**(1), 143–153.

Bhowmik P., and Nandy D., 2018, Prediction of the strength and timing of sunspot cycle 25 reveal decadal-scale space environmental conditions: Nature Communications, **9**(1), 1–10.

Chen, Y., Zhang, Y., Wang, Y. D., et al., 2018, Co-seismic responses of fluid observation data in Gansu area during the Nepal M8.1 earthquake: China Earthquake Engineering Journal, **40**(S1), 90–94.

Chen, Y.T., 2009, Earthquake prediction: retrospect and prospect: Scientia Sinica (Terrage), **39**(12), 1633–1658.

Cristo, A., Vaquero, J. M., and Sánchez-Bajo, F., 2011, Hsunspots: A tool for the analysis of historical sunspot drawings: Journal of Atmospheric and Solar-terrestrial Physics, **73**(2–3), 187–190.

Cui, X. J., Yan, J. P., Dong, Z. B., et al., 2013, The active pattern and future trend of earthquakes with Ms≥7 in Philippines in recent 50 years: South China Journal of Seismology, **33**(2), 47–54.

Deng, Q. D., Feng, X. Y., and Zhang, P. Z., 2000, Tianshan active structure: Seismological Press, Beijing, **75**.

Eck, N. J. V., and Waltman, L., 2009, How to normalize co-occurrence data? An analysis of some well-known similarity measures: Journal of the American society for information science and technology, **60**(8), 1635–1651.

Egghe, L., 2009, New relations between similarity measures for vectors based on vector norm: Journal of the American Society for Information Science and Technology, **60**(2), 232–239.

Fang, W., Liu, C., Zhang, C. S., et al., 2003, Relationship between the sunspots and strong earthquakes in the world: Earthquake Research in Plateau, **15**(4), 27–31.

Feng, X. Y., 1986a, Active fault and seismic in Tianshan Mountains: Xinjiang Geology, **4**(3), 100–106.

Feng, X. Y., 1986b, The active faults in Tianshan Mountains: Earthquake Research in China, **2**(2), 84–89.

Guilherme W. S. De Melo, and Aderson F. Do Nascimento., 2018, Earthquake magnitude relationships for the Saint Peter and Saint Paul Archipelago, Equatorial Atlantic: Pure and Applied Geophysics, **175**(3), 741–756.

Guo, A. N., Guo, Z. J., Ren, D., et al., 2016, Retrospective discussion of prediction by using non-traditional method for the 2013 Minxian-Zhangxian Ms6.6 earthquake in Gansu: South China Journal of Seismology, **36**(2), 56–59.

Guo, Z. J., and Guo, A. N., 2017, Discussion on the medium-term prediction of Jiuzhaigou, Sichuan Ms7.0 earthquake on August8, 2017, by means of triplet method: China Earthquake Engineering Journal, **39**(4), 0797–0798.

Guo, Z. J., Guo, A. N., Li, Y. R., et al., 2006, Discussion on retrospective prediction of 1966 Xingtai large earthquake: Inland Earthquake, **20**(2), 97–101.

Hu, M. S., 2013, Data mining and modeling from historical disaster: China Water Power Press, Beijing.

Hu, H., and Han, Y. B., 2005, Prediction of the Hualian earthquakes in Taiwan and an extended discussion on the method of commensurability: Applied Geophysics, **2**(3), 194–196.

Hu, M. S., Jia, Z. J., Ji, X. Y., et al., 2014, A method of co-occurrence frequency analysis to find out correlations among earthquake areas: Computer Engineering & Science, **36**(3), 536–540.

Jiang, B. Q., 2018, The relationship between sunspot, magnetic storm and seismic activity: Acta Seismologica Sinica, **7**(4), 452–460.

Li, C. L., 2019, Re-estimate of Major Earthquake Activity in Surrounding Areas after the MS 6.6 Jinghe Earthquake in Xinjiang, 2017: Pure and Applied Geophysics, **176**(2), 563–576.

Liu, Y. L., and Yan, J. P., 2015, The model and effect test about the trend judgment of natural disasters: Journal of Shaanxi Normal University, **43**(5), 96–102.

Long, X. X., Yan, J. P., Sun, H., et al., 2006, Study on earthquake tendency in Sichuan-Yunnan region based on commensurability: Journal of Catastrophology, **21**(3), 81–84.

Lv, N. D., and Zhang, Q., 1996, Theory of forecasting: Petroleum Industry Press, Beijing, 21–22.

Meng, Z. T., Liu, J. W., Xie, Z. J., et al., 2021, Analysis of the correlation between the temporal-spatial distribution of b-value and seismic hazard: a review: Progress in Geophysics, **36**(1), 30–38.

Morillo, F., Bordons, M., and Gómez, I., 2003, Interdisciplinarity in science: A tentative typology of disciplines and research areas: Journal of the American Society for Information Science and technology, **54**(13), 1237–1249.

Qiang, Z. J., Yao, Q. L., Wei, L. J., et al., 2008, The annular stress thermal field of satellite thermal infrared prior earthquakes: Acta Geoscientica Sinica, **29**(4), 486–494.

Qin, S. Q., Xiong, J. H., Xue, L., et al., 2011, Seismologic law and mode of strong earthquake: Journal of Earth Sciences and Environment, **33**(3), 311–316.

Salton, G., and McGill, M. J., 1983, Introduction to modern information retrieval: McGraw-Hill, London.

Shan, B., Xiong, X., Zheng, Y., et al., 2013, Stress changes on major faults caused by 2013 Lushan earthquake and its relationship with 2008 Wenchuan earthquake: Science China Earth Sciences, **56**(7), 1169–1176.

Song, Z. P., Zhang, G. M., Liu, J., et al., 2011, Global earthquake catalog (9999 B.C.–1963 A.D. M≥5.0,1964 A.D.–2010 A.D. ≥5.0): Seismological Press, Beijing.

Tu, X. X., Wang, H. Y., Wang, J., et al.,2019, Geomagnetic anomalies prior to the Minxian–Zhangxian M6.6 earthquake of 2013: China Earthquake Engineering Journal, **41**(6), 1568–1573.

Wang, H., Yan, J. P., Tang, B. Q., et al., 2018, Space-time symmetry and tendency judgment of Mw≥6.9 earthquake in Peru: Journal of Zhejiang University (Science Edition), **45**(1), 1–9.

Wei, L. J., Guo, J. F., Cai, H., et al., 2008, Satellite thermal infrared anomaly: a short term and impending earthquake precursor before the Wenchuan Ms8.0 earthquake in Sichuan, China: Acta Geoscientica Sinica, **29**(5), 583–591.

Weng, W. B., 1984, Fundamentals of forecasting theory: Petroleum Industry Press, Beijing.

World Economic Forum, 2020, The global risks report 2020: Davos, Marsh & McLennan and Zurich Insurance Group, Switzerland.

Wu, Q., and Cao, M. T., 2018, A preliminary study on the correlativity of seismic hazard between Beijing area and Xiong'an new area: Seismolgy and Geology, **40**(4), 935–943.

Wu, Y. J., Zhang, P., Di, J. R., et al., 2010, Study on bipartite networks: Complex Systems and Complexity Science, **7**(1): 112.

Yan, J. P., 2013, Study on space-time symmetry of major natural disasters: Shaanxi Normal University Publishing House Co Ltd, Xi'an.

Yan, J. P., 2016, Space-time symmetry of earthquakes: Science Press Ltd, Beijing.

Yin, J. Y., Zhu, Y. Q., Song, Z. P., et al., 2011, Hundred-year-scale cycle of seismic activities in western China and its negative correlativity with sunspot activity: Chinese Journal of Geophysics, **54**(9), 2263–2271.

Zhang, L. L., Dong, J., Yan, J. P., et al., 2012, The symmetry and the tendency judgment of Ms≥6.6 earthquakes in southern Tibet: Plateau Earthquake Research, **24**(3), 1–5.

Wan Jia is a Ph.D. student at the School of Geography and Tourism, Shaanxi Normal University, Xi'an. She obtained a master's degree from Shaanxi Normal University in 2013. Her research interests are regional sustainable development and disaster prevention. E-mail:wanjia3963@126.com.

Corresponding author: Yan Jun-Ping is a professor and doctoral supervisor working at the School of Geography and Tourism, Shaanxi Normal University, Xi'an. He obtained his doctor's degree from Xi'an University of Technology in 2003. He has led a number of projects funded by the National Natural Science Foundation of China. At present, his research interests are global change and natural disaster prevention.
E-mail: yanjp@snnu.edu.cn.